Journal of Food Engineering 153 (2015) 96–107

Contents lists available at ScienceDirect

Journal of Food Engineering

journal homepage: www.elsevier.com/locate/jfoodeng

Effect of the number of orifices and operative variables on the heat and mass transfer in a hydrofluidization system with static spheres

Eliana E. Belis, Susana E. Zorrilla, Juan M. Peralta *

Instituto de Desarrollo Tecnológico para la Industria Química (INTEC), Universidad Nacional del Litoral – CONICET, Güemes 3450, S3000GLN Santa Fe, Argentina

ARTICLE INFO

Article history:
Received 19 August 2014
Received in revised form 17 December 2014
Accepted 18 December 2014
Available online 26 December 2014

Keywords:
Hydrofluidization
CFD
Food
Heat transfer
Mass transfer

ABSTRACT

Hydrofluidization is a method of chilling and/or freezing that uses submerged jets of a refrigerating liquid. The objective of this work was to study the effect of refrigerant temperature (−5 °C, −10 °C), fluid velocity at the jet exit (1.18 m s^{-1}, 2.36 m s^{-1}), distance between adjacent jets (1 cm, 2 cm), and distance between spheres and jet exit (1 cm, 5 cm) on the heat and mass transfer in a hydrofluidization system (*e.g.* heat transfer coefficient, turbulence intensity, solute concentration in the food) with several static spheres using a previously developed and validated mathematical model *via* CFD simulations. The variables that most affected the transport phenomena in the fluid domain were the distance between spheres and jet exit, the distance between adjacent jets, the fluid velocity at the jet exit, and the distance between spheres. The refrigerant temperature only had significant effect on the transport phenomena inside the food samples.

1. Introduction

Hydrofluidization (HF) can be defined as a method of chilling and/or freezing that uses a circulating system for pumping a refrigerating liquid upwards through orifices or nozzles into a vessel full with the refrigerating media. Thus, submerged agitating jets are created ensuring extremely high surface heat transfer coefficients (Fikiin, 1992, 2008). As a technique derived from the immersion chilling and freezing (ICF) method, HF shares some of its advantages such as: fast freezing method, energy-saving and environmentally-friendly technology, capacity to formulate desired final products by controlling the mass transfer during processing (addition of micronutrients, flavoring, antioxidants, etc.) (Fikiin, 2008; Peralta et al., 2009).

The effect of some of the operative variables of a HF system on the transport phenomena between the refrigerant and the food samples has been subject of study by several research groups over the recent decades (Fikiin, 1992; Verboven et al., 2003; Peralta et al., 2007, 2009, 2010, 2012). Those studies were carried out experimentally and/or theoretically and helped to identify some of the main variables that influence the heat and mass transfer during processing such as the refrigerant velocity at the orifices (or flow rate), the temperature and the food size. In general, the complexity of combining the study of the transport phenomena in the fluid and food system with the phase change phenomenon makes the mathematical modeling a very difficult problem to tackle. Some of the main contributions using the simplest and idealized HF configuration (*i.e.* single sphere and single jet) were developed using computational fluid dynamic (CFD) simulations (Peralta et al., 2010, 2012). These studies presented a validated mathematical model to estimate the heat and mass transfer inside a food sample with a regular geometry during its freezing and using a simplified configuration of a hydrofluidization system.

Nevertheless, the effects on the transport phenomena of some important parameters that are related to the geometry of the system were not studied, such as the number of the orifices that produce the jets and the number of the food samples (Peralta et al., 2012). The objective of this work was to study the effect of the operative variables (refrigerant temperature, average velocity of the refrigerant fluid at the orifices, distance between the plane of the orifice plate and the stagnation point of the spheres, distance between the geometrical centers of the round orifices and the distance between the geometrical centers of the spheres) on the heat and mass transfer in a hydrofluidization system with several static spheres and round jets using a previously developed and validated mathematical model *via* CFD simulations.

2. Materials and methods

2.1. System studied

The studied hydrofluidization system consisted in a cylindrical vessel of 100 mm diameter and 100 mm height and a plate with

* Corresponding author. Tel.: +54 342 451 1595; fax: +54 342 451 1079.
E-mail address: jmperalta@intec.unl.edu.ar (J.M. Peralta).

http://dx.doi.org/10.1016/j.jfoodeng.2014.12.016
0260-8774/

Nomenclature

A_y	cross sectional area to the domain axis at the height y (m^2)
$a_{i,j}$	fitting coefficients of Eq. (5) (–)
C_{NaCl}	average NaCl concentration in the potato spheres ($g\ kg^{-1}$)
C_p	heat capacity of the fluid ($J\ kg^{-1}\ K^{-1}$)
Cp	pressure coefficient calculated using Eq. (2) (–)
Cp_{CFD}	pressure coefficient obtained from simulations ($p/(1/2\rho V^2)$) (–)
D	diameter of the spheres (cm)
d	diameter of the orifices (cm)
H	distance between the orifice plate and the plane of the stagnation points of the spheres (cm)
h_c	surface heat transfer coefficient obtained from Eq. (1) ($W\ m^{-2}\ K^{-1}$)
$h_{c,CFD}$	surface heat transfer coefficient obtained from simulations ($W\ m^{-2}\ K^{-1}$)
$h_{c,stg}$	averaged values of h_c evaluated on $\varphi = 0$ for all spheres ($W\ m^{-2}\ K^{-1}$)
h_c^*	averaged surface heat transfer coefficient (Peralta et al., 2009) ($W\ m^{-2}\ K^{-1}$)
k	thermal conductivity of the fluid ($W\ m^{-1}\ K^{-1}$)
L	distance between the geometric centers of the spheres (cm)
L_y	curve on the surfaces of the spheres at height y (m)
Nu_{ave}	average Nusselt number based on h_c^* ($h_c^* D/k$) (–)
Nu_{stg}	stagnation-point Nusselt number based on $h_{c,stg}$ ($h_{c,stg} D/k$) (–)
Pr	Prandtl number ($\mu C_p/k$) (–)
p	pressure (Pa)
R	radius of the spheres (m)
Re	Reynolds number ($\rho DV/\mu$) (–)
r	radial position (m)
S	distance between the geometric center of the orifices (cm)
T	temperature of the refrigerant fluid (°C)
T_c	temperature of the geometric center of the spheres (°C)
t	time (s)
t_R	relative freezing time (–)
Tu	turbulence level calculated from Eq. (3) (–)
Tu_{CFD}	turbulence level obtained from the simulations ($\sqrt{2/3\kappa}/v$) (–)
V	area averaged fluid velocity at the orifices ($m\ s^{-1}$)
V_T	volume of the fluid domain (m^3)
v	fluid velocity ($m\ s^{-1}$)
y	axial position in the fluid domain (m)
y^+	dimensionless distance on the sphere walls (–)

Greek symbols

θ	polar position (grad)
κ	turbulence kinetic energy ($m^2\ s^{-2}$)
μ	viscosity of the fluid (Pa s)
ρ	density of the fluid ($kg\ m^{-3}$)
φ	azimuth position (grad)

different number of 3 mm diameter round orifices (to produce the jets) in its base (Fig. 1). This system is a smaller version of the one studied by Peralta et al. (2009, 2010, 2012). A regularly spaced squared array of 20 mm diameter static spheres placed at different distances from the orifice plate was used. Fig. 2 shows the orifice and sphere arrays studied. The spheres were considered made by copper for the determination of the surface heat transfer coefficient and made by potato (*Solanum tuberosum* L.) to model the heat and mass transfer in a food sample. An aqueous solution of NaCl was considered to model the refrigerant solution (with a concentration of 0.231 $kg\ kg^{-1}$ (w/w)) and the occluded solution in the food sample.

2.2. Operative conditions and geometric arrays studied

A combination of thermal, flow and geometric variables were tested. Those variables were: the refrigerant temperature ($T = -5$ °C and $T = -10$ °C), the average velocity of the refrigerant fluid at the orifices ($V = 1.18\ m\ s^{-1}$ and $V = 2.36\ m\ s^{-1}$), the distance between the plane of the orifice plate and the stagnation point of the spheres ($H = 1$ cm and $H = 5$ cm), the distance between the geometrical centers of the round orifices ($S = 1$ cm and $S = 2$ cm) and the distance between the geometrical centers of the spheres ($L = 2$ cm and $L = 6$ cm). It is worth mentioning that $L = 6$ cm allows representing a single sphere placed at the domain axis (Fig. 2). The 32 conditions studied are shown in Table 1, including their codification.

2.3. Mathematical modeling of the transport phenomena

The transport phenomena that take place in the studied system were estimated using a mathematical model for the conditions proposed in Table 1. Heat, mass and momentum transfer balances were solved for the refrigerant liquid domain, and heat and mass transfer balances were solved for the food sample. In all cases, numerical methods were used to solve the proposed balances, due to the high nonlinear nature of the mathematical expressions.

2.3.1. Heat and momentum transfer in the liquid refrigerant

2.3.1.1. Mathematical model. The momentum (Navier–Stokes), mass (continuity) and energy transfer in the refrigerant liquid domain was simulated using the mathematical model proposed by Peralta et al. (2010) for a hydrofluidization system. The model

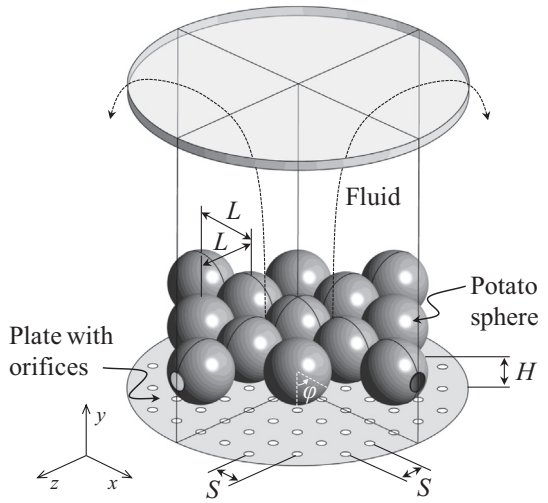

Fig. 1. Schematic diagram of the hydrofluidization system studied.

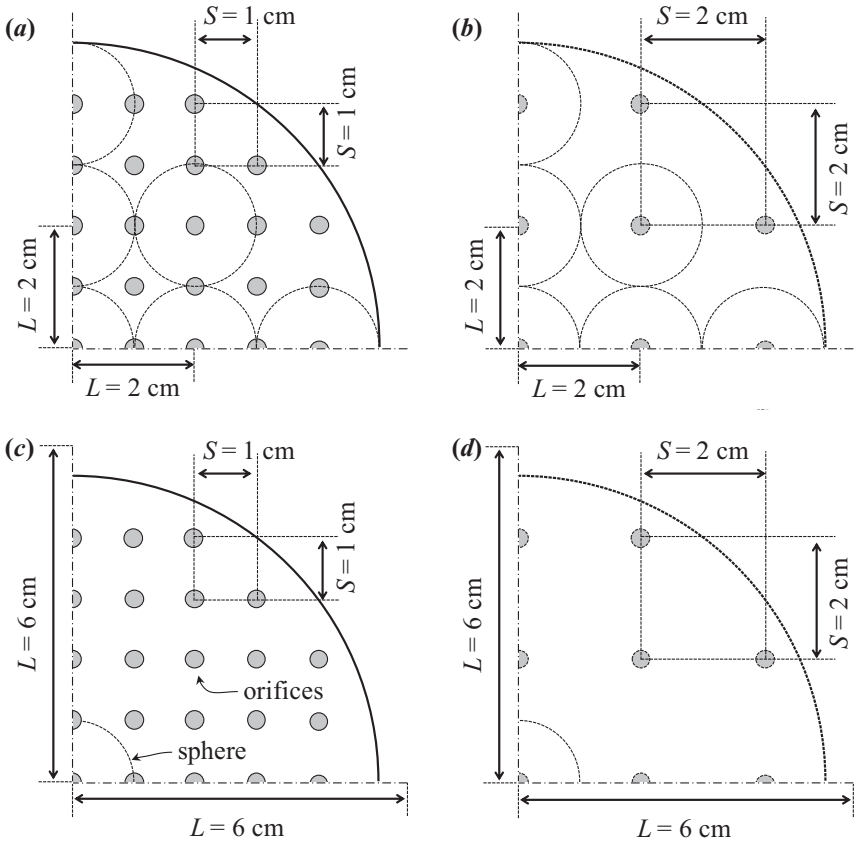

Fig. 2. Top view of the orifice and sphere arrays (square) used for the simulations. (a) S = 1 cm (69 orifices) and L = 2 cm (13 spheres), (b) S = 2 cm (21 orifices) and L = 2 cm (13 spheres), (c) S = 1 cm (69 orifices) and L = 6 cm (1 sphere), and (d) S = 2 cm (21 orifices) and L = 6 cm (1 sphere).

Table 1
Studied conditions with their codification.

T = −5 °C					T = −10 °C				
V (m s^{-1})	H (cm)	S (cm)	L (cm)	Code	V (m s^{-1})	H (cm)	S (cm)	L (cm)	Code
1.18	1	1	2	T5V118H1S1L2	1.18	1	1	2	T10V118H1S1L2
			6	T5V118H1S1L6				6	T10V118H1S1L6
		2	2	T5V118H1S2L2			2	2	T10V118H1S2L2
			6	T5V118H1S2L6				6	T10V118H1S2L6
	5	1	2	T5V118H5S1L2		5	1	2	T10V118H5S1L2
			6	T5V118H5S1L6				6	T10V118H5S1L6
		2	2	T5V118H5S2L2			2	2	T10V118H5S2L2
			6	T5V118H5S2L6				6	T10V118H5S2L6
2.36	1	1	2	T5V236H1S1L2	2.36	1	1	2	T10V236H1S1L2
			6	T5V236H1S1L6				6	T10V236H1S1L6
		2	2	T5V236H1S2L2			2	2	T10V236H1S2L2
			6	T5V236H1S2L6				6	T10V236H1S2L6
	5	1	2	T5V236H5S1L2		5	1	2	T10V236H5S1L2
			6	T5V236H5S1L6				6	T10V236H5S1L6
		2	2	T5V236H5S2L2			2	2	T10V236H5S2L2
			6	T5V236H5S2L6				6	T10V236H5S2L6

was solved using CFD and assuming the fluid as Newtonian. The turbulence phenomenon was taken into account using the two parameter model κ–ω Shear Stress Transport (SST) (Wilcox, 2006) due to its capacity to predict flows over curved surfaces and boundary layer detachments (Olsson et al., 2004).

2.3.1.2. Computational domain and conditions of the simulations. A 90° cylindrical portion (Fig. 3) of the physical domain showed in Fig. 1 was considered as the computational domain in order to reduce computational efforts. The fluid exit was considered as a 3 mm width slit placed at the top of the cylindrical wall of the domain (Peralta et al., 2010). A free slip wall was used in the top of the domain at the air–liquid interface. The spheres were assumed to be made by copper and their initial temperature was 20 °C.

The computational domain (liquid and copper) was discretized by using a mesh composed by tetrahedral and several layers of prisms near the sphere–fluid interface (in both sides). To improve the prediction capacity using the same computational requirements, the density of the mesh was higher in the zone near the orifices and the surfaces of the spheres and lower in the rest of the domain. The solid walls were assumed to be adiabatic (except at

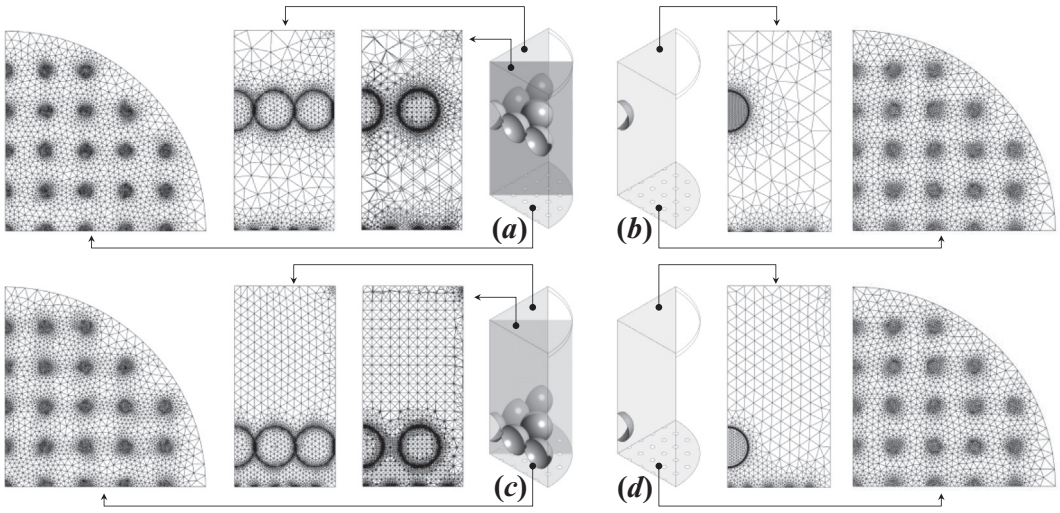

Fig. 3. Side view showing the meshes used for simulations. (a) $L = 2$ cm and $H = 5$ cm, (b) $L = 6$ cm and $H = 5$ cm, (c) $L = 2$ cm and $H = 1$ cm, and (d) $L = 6$ cm and $H = 1$ cm.

the spheres) and the total system pressure was 0.1 MPa. The velocity profile of the liquid refrigerant at the orifices was modeled by using a 1/7th type expression and the turbulence intensity at each orifice was assumed to be 5% (Geers et al., 2004; CFX, 2006).

Each condition was simulated up to 2 s because a quasi-steady state was reached in the fluid flow field and in the surface heat transfer coefficient profiles (data not shown).

The mass and heat transfer balance equations were solved (pre-processing, solving and post-processing) by using the commercial CFD software ANSYS-CFX 14.1 (Ansys Inc., Canonsburg, USA). The computational domain and the mesh were obtained using ANSYS-ICEM-CFD 14.1 (Ansys Inc., Canonsburg, USA). Simulations were carried out using: (i) a PC Intel Pentium 4 3.2 GHz with 2 GB of RAM (DDR2 533 MHz) for the cases where $L = 6$ cm and (ii) a PC Intel core i7 3930 of 3.2 GHz with 16 GB of RAM (DDR3 1600 MHz) for the cases where $L = 2$ cm. Each simulation took approximately 4 h to converge in the cases of $L = 6$ cm (1 sphere) and 15 h in the cases of $L = 2$ cm (13 spheres).

2.3.1.3. Variables analyzed. CFD simulations can produce a large amount of information about the transport phenomena that take place in this type of systems. To facilitate the analysis and future comparisons with experimental data, representative variables were conveniently selected to study the heat and mass transfer. These variables were: local surface heat transfer coefficient (h_c), average heat transfer coefficient (h_c^*) calculated by using a lumped capacitance method (Peralta et al., 2009), average stagnation-point heat transfer coefficient ($h_{c,stg}$), pressure coefficient (Cp), the area-averaged turbulence intensity for different heights in the domain (Tu) and the volume-averaged turbulence intensity ($\langle Tu \rangle$). Also, velocity contours and streamlines for the conditions studied were obtained at $t = 2$ s.

The variables h_c, Cp, Tu, $\langle Tu \rangle$ were determined through the variables studied by Peralta et al. (2010) using the following expressions:

$$h_c(\varphi) = \frac{1}{L_y}\int_{L_y} h_{c,CFD}\,dL_y \tag{1}$$

$$Cp(\varphi) = \frac{1}{L_y}\int_{L_y} Cp_{CFD}\,dL_y \tag{2}$$

$$Tu(y) = \frac{1}{A_y}\int_{A_y} Tu_{CFD}\,dA_y \tag{3}$$

$$\langle Tu \rangle = \frac{1}{V_T}\int_{V_T} Tu_{CFD}\,dV_T \tag{4}$$

where L_y is the curve on the surface of the spheres at a position y (*i.e.* latitude), A_y is the transversal surface to the fluid domain axis at a position y, V_T is the total volume of fluid in the domain, $h_{c,CFD}$ is the local surface heat transfer coefficient (function of θ and φ) obtained from the simulations, Cp_{CFD} is the pressure coefficient (function of θ and φ) obtained from the simulations, Tu_{CFD} is the local turbulence intensity (function of x, y and z) obtained from the simulations. Also, $h_{c,stg}$ was obtained by averaging arithmetically the values of $h_c(\varphi = 0)$ for all spheres.

2.3.1.4. Nusselt correlation. The most common way to condensate transport phenomena information of a particular system is to use a correlation considering the representative dimensionless numbers. The average surface heat transfer coefficient h_c^* and the average stagnation heat transfer coefficient $h_{c,stg}$ were correlated to the operative conditions using an empirical correlation. Taking into account the analysis presented by Peralta et al. (2009) and Tie et al. (2011) to correlate the heat transfer information to the operative and geometric variables of their studied systems, the following expression was assumed:

$$Nu_j = a_{1,j} Re^{a_{2,j}} Pr^{a_{3,j}} (H/d)^{a_{4,j}} (S/d)^{a_{5,j}} (L/d)^{a_{6,j}} \tag{5}$$

where Nu_j is the average ($j = ave$) Nusselt number based on h_c^*, or the stagnation-point ($j = stg$) Nusselt number based on $h_{c,stg}$, Re in the Reynolds number, Pr is the Prandtl number, H/d is the dimensionless distance between the orifice plate and the plane of the stagnation points of the spheres, S/d is the dimensionless distance between the geometrical centers of the orifices, L/d is the dimensionless distance between the geometrical centers of the spheres and $a_{i,j}$ are the fitting coefficients.

The coefficients $a_{i,j}$ were found by a fitting procedure comparing the values of the calculated (Eq. (5)) and simulated Nu_j. The procedure was carried out minimizing the objective function using a non-linear fitting procedure implemented in the statistical software Minitab 13.20 (Minitab Inc., State College, PA). The objective function was:

$$Obj = \sqrt{\sum_{l=1}^{n} \frac{(Nu_{sim,l} - Nu_{corr,l})^2}{n}} \tag{6}$$

where n is the number of studied conditions, $Nu_{sim,l}$ is the Nusselt number obtained from the CFD simulations for the lth condition and $Nu_{sim,l}$ is the Nusselt number obtained from Eq. (5) for the lth condition.

Table 2
Composition of the meshes used in this study.

L (cm)	H (cm)	Fluid		Spheres		Total
		Tetrahedra	Prisms	Tetrahedra	Prisms	
6	1	95528	21494	18246	8764	144032
6	5	106548	26642	18246	8764	160200
2	1	392191	289472	244222	183560	1109445
2	5	392250	290000	244181	183025	1109456

2.3.2. Heat and momentum transfer in the food sample

2.3.2.1. Mathematical model. Heat and mass transfer inside the food sample was estimated using the mathematical model developed by Zorrilla and Rubiolo (2005a, 2005b) and extended to spherical geometries by Peralta et al. (2012). This model uses a volume averaging approach to the discontinuities of the heterogeneous system (occluded solution, ice and solid matrix) that represents the food sample. A pseudo homogeneous and continuous system is obtained and differential heat and mass transfer balances are applied (Peralta et al., 2012). In addition, to estimate the fields of temperature and concentration, the fraction of water that is frozen and unfrozen is predicted at each point within the food considering thermodynamic equilibrium between the occluded solution and ice phases (Zorrilla and Rubiolo, 2005a, 2005b).

2.3.2.2. Computational domain and conditions of the simulations. The computational domain was a representative sphere of 20 mm diameter. Thermophysical properties of potato were used (Peralta et al., 2012).

The balances were applied in spherical coordinates taking into account a two dimensional system in transient conditions. These balances were solved using a finite difference method. The discretization of the food domain was performed by using a 3D mesh composed by 1800 hexahedral elements using 30 steps in r direction and 60 steps in φ direction. A logarithmic discretization was used in r direction due to the main changes occur near the interface food-refrigerant (Peralta et al., 2012). The numerical scheme was implemented in a computer program using Fortran language (Compaq Visual Fortran 6.1, Compaq Computer Corporation, Houston, USA and Intel Visual Fortran Composer XE 2013, Santa Clara, USA) (Peralta et al., 2012). The numeric scheme was solved, as for the case of the refrigerant domain, using: (i) a PC Intel Pentium 4 of 3.2 GHz with 2 Gb RAM (DDR2 533 MHz) for the cases with domains containing 1 sphere, and (ii) a PC Intel core i7 3930 of 3.2 GHz with 16 Gb RAM (DDR3 1600 MHz) for the cases with domains containing 13 spheres. Each condition was simulated up to 1800 s and took approximately 10 h (in domains with 1 sphere) and 24 h (in domains with 13 spheres) to converge.

2.3.3. Connection between the fluid and food domains

The balances were solved by decoupling the momentum from energy and mass transfer. This procedure was carried out taking into account the difference in orders of magnitude (approximately 2) between the transfer rate of momentum and energy or mass (Peralta et al., 2010, 2012).

The surface heat transfer coefficient profile (h_c) was used as the variable that carries the information of the transfer phenomena between the refrigerant fluid and the food sample. This transference of information was performed using the following procedure: (a) the energy transfer and continuity balances were solved in the liquid refrigerant for each condition using copper spheres (Peralta et al., 2010, 2012), (b) surface heat transfer coefficient (h_c) based on Eq. (1) for each studied condition was obtained, and finally (c) the values of h_c were used as a boundary condition in the modeling of the heat and mass transfer in food samples. The mass transfer at the surface of the spheres was estimated using the Chilton–Colburn analogy and the calculated h_c profiles (Peralta et al., 2012).

2.3.4. Model validation

The mathematical models used in this work were validated in previous studies (Peralta et al., 2010, 2012) on a similar hydrofluidization system. Thus, the validation step was omitted in this study.

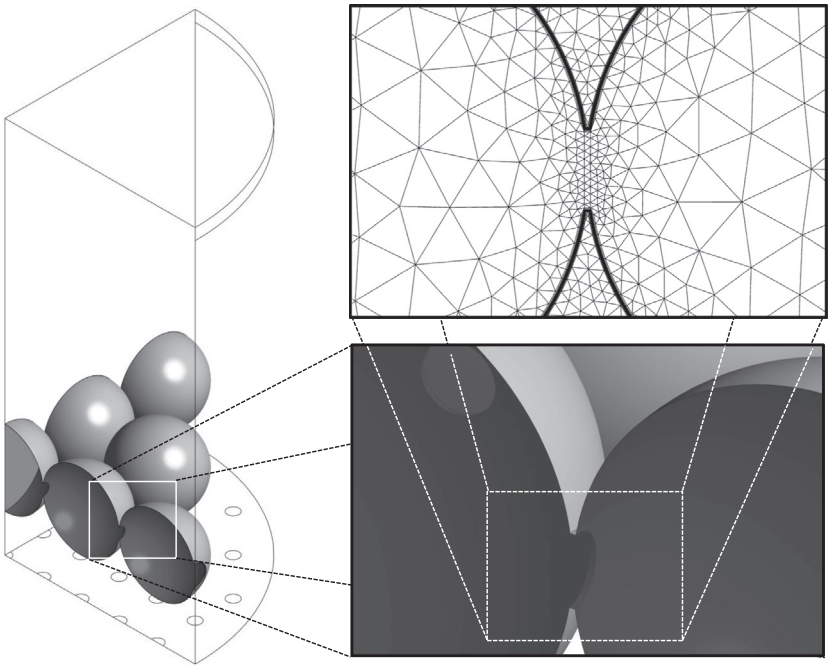

Fig. 4. Detail of the connections between the spheres used for the meshes when L = 2 cm.

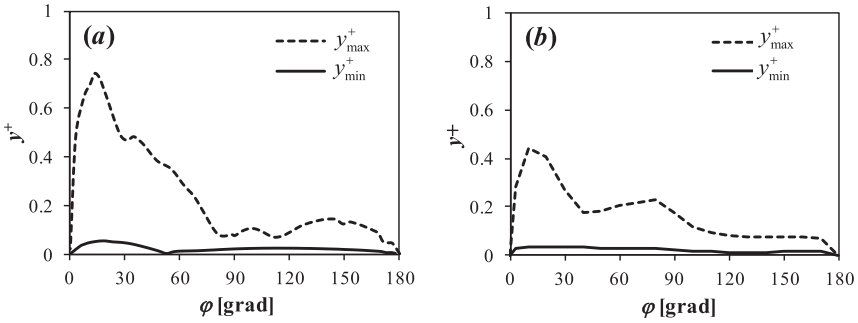

Fig. 5. Profiles of y^+ (maximum and minimum) as a function of the angular position on the sphere surfaces for the conditions: (a) domains with L = 6 cm and (b) domains with L = 2 cm.

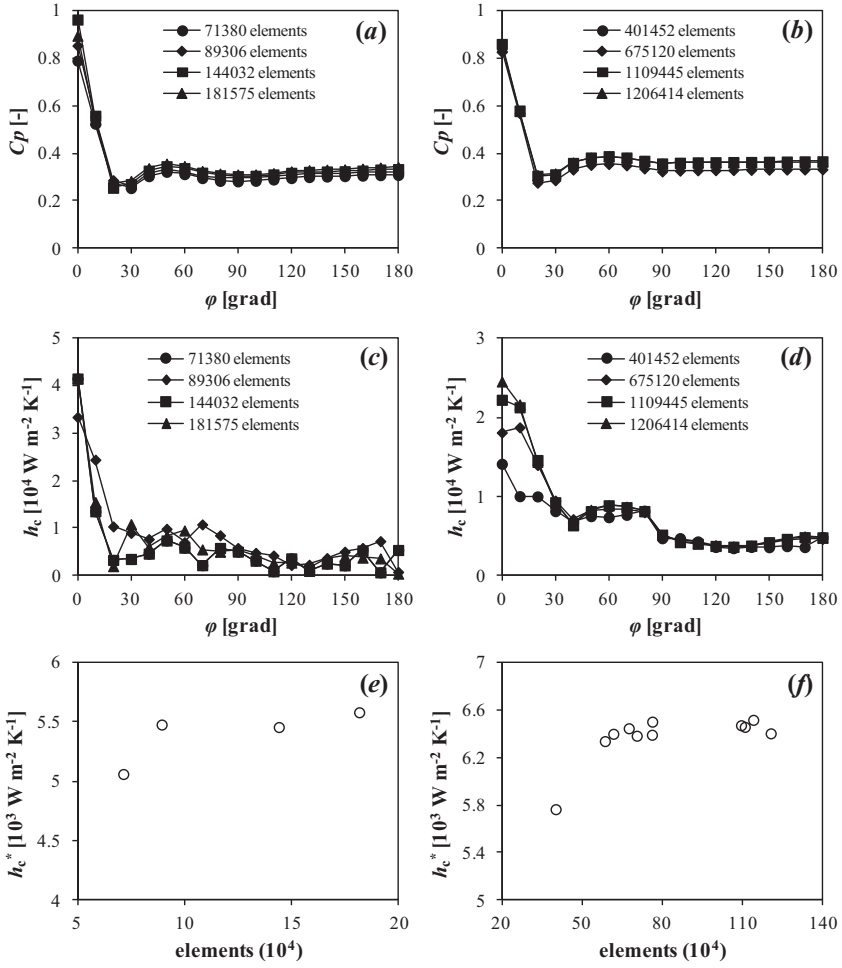

Fig. 6. Mesh independence. Local values of (a) Cp (L = 6 cm), (b) Cp (L = 2 cm), (c) h_c (L = 6 cm), (d) h_c (L = 2 cm), (e) h_c^* (L = 6 cm), and (f) h_c^* (L = 2 cm).

3. Results and discussion

3.1. Heat and momentum transfer in the refrigerant domain

3.1.1. Mesh independence test

The mesh independence was tested using the local values of h_c, Cp and h_c^*. Four mesh compositions were selected and used based on the tests performed (Table 2). It is important to mention that for meshes with L = 2 cm, the contact point between the spheres were modeled using a small cylinder as a connector (Fig. 4) (Kuroki et al., 2009) to minimize the problems in the mesh quality and subsequently in convergence arisen from the elements near those points. Also, the y^+ parameter was verified to be less than 1 in all cases (CFX, 2006) (Fig. 5). Finally, the local values of h_c, Cp and h_c^* as a function of the element number for the evaluated meshes are shown in Fig. 6.

3.1.2. Velocity contours and streamlines

The velocity contours along with their respective streamlines for the conditions studied are shown in Fig. 7. Only the results for V = 2.36 m s^{-1} are presented due to the similarity in the morphology with the results for V = 1.18 m s^{-1}. It is important to note that the velocity contours and the streamlines shown in Fig. 7 are

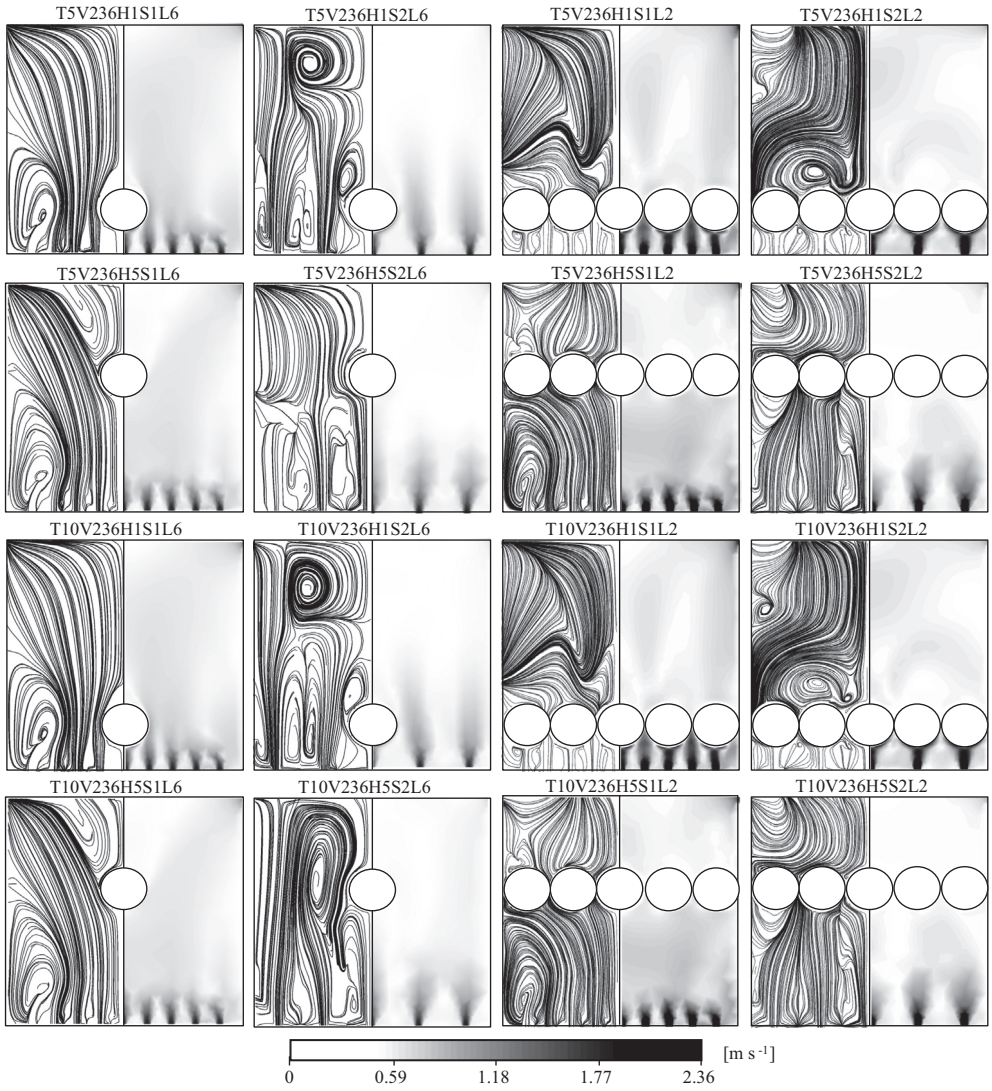

Fig. 7. Streamlines and velocity contours for the selected conditions when $V = 2.36$ m s^{-1}.

evaluated on a representative cut plane (*i.e.* plane *xy* with $z = 0$ m) of the domain for 2 s of simulation.

Fig. 7 shows the velocity contours for $L = 6$ cm. In general, an increment in the number of orifices produced an increment in the local velocities in the domain. This behavior was most noticeable in the zone where the jets were formed and near the sphere surface. The streamlines showed that more separated jets (*i.e.* fewer orifices) produced more interaction among jets and larger recirculation zones after and before the spheres. This behavior was more evident towards the central axis of the domain. A similar jet–jet interaction pattern in the zone between the orifices and the sphere is observed for multiple submerged jets impinging on a flat surface (Geers et al., 2004, 2005; Draksler et al., 2014). Conversely, an increase in the number of orifices produced less perturbed jets. This could be explained due to the existence of a more uniform fluid field with high local velocities and lower velocity gradients. On the contrary, fewer orifices produce a less intense and more cyclic fluid stream due to the jet interaction which would produce premature boundary layer separation. It is noteworthy that it was observed a periodically appearance and disappearance of eddies in the domain in the zone between the sphere and the exit of the domain.

Similarly to conditions with $L = 6$ cm, an increase in the orifice number produced higher local velocities for conditions with $L = 2$ cm. The streamlines shows larger recirculation zones in the region between the orifices and the forward stagnation points of the spheres as S and H increased. Those zones were less disturbed near the main axis of the domain, possibly due to its central position in the domain (*i.e.* less disturbed by domain walls). Again, a periodic behavior was observed for the jet wakes behind the spheres for all conditions. This periodic performance was less frequent for $H = 5$ cm maybe due to the smaller fluid volume between the rear stagnation points of the sphere and the fluid–air interface.

In both cases ($L = 6$ cm and $L = 2$ cm), the refrigerant temperature did not affect significantly the velocity contours and the streamlines. This could be due to the small difference between the selected values.

3.1.3. Turbulence levels

Turbulence levels (Tu) as a function of the axial position and for all conditions are shown in Fig. 8. In general, the Tu profiles showed initially an increase from the initial value (*i.e.* $Tu_0 = 0.05$) at the orifices and then a plateau and/or a slowly decrease or increment as the fluid moves through the domain to the exit. A similar result is presented in literature for Tu evaluated in the axis of a single submerged jet (Deo et al., 2007; Ball et al., 2012). This could be explained firstly because typically the jet cores could survive approximately a distance of $y/H = 3$ to 10 (*i.e.* $y \cong 0.01$–0.03 m)

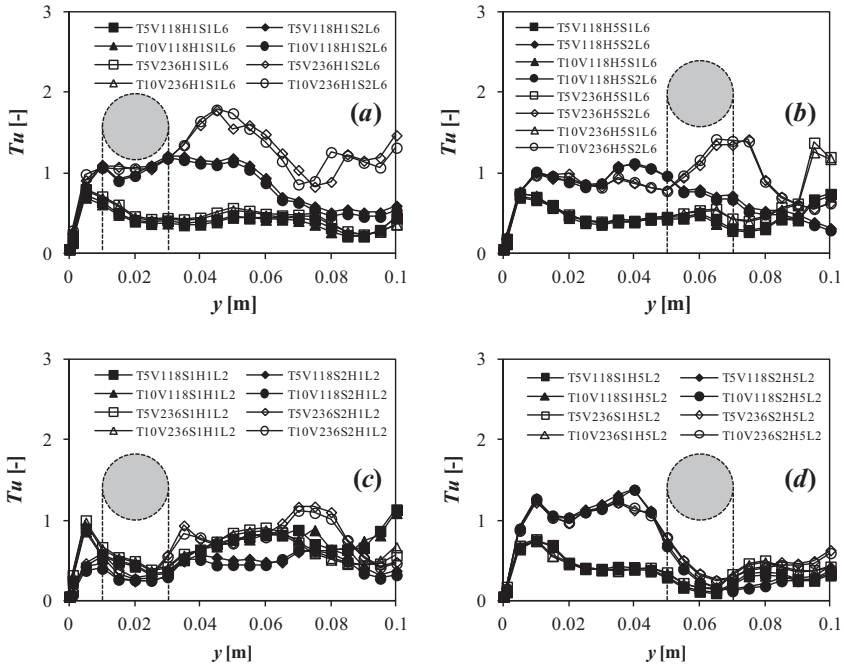

Fig. 8. Turbulence levels (Tu) as a function of the axial position y. (a) L = 6 cm and H = 1 cm, (b) L = 6 cm and H = 5 cm, (c) L = 2 cm and H = 1 cm, and (d) L = 2 cm and H = 5 cm. The sphere marks the axial position of the plane that forms the sphere arrangement.

Table 3
Values of $\langle Tu \rangle$ for the studied conditions.

Condition	$\langle Tu \rangle$ (–)	Condition	$\langle Tu \rangle$ (–)
T5V118H1S1L6	0.407	T10V118H1S1L6	0.383
T5V118H1S2L6	0.825	T10V118H1S2L6	0.787
T5V118H5S1L6	0.435	T10V118H5S1L6	0.419
T5V118H5S2L6	0.731	T10V118H5S2L6	0.706
T5V236H1S1L6	0.451	T10V236H1S1L6	0.433
T5V236H1S2L6	1.184	T10V236H1S2L6	1.192
T5V236H5S1L6	0.545	T10V236H5S1L6	0.535
T5V236H5S2L6	0.906	T10V236H5S2L6	0.916
T5V118H1S1L2	0.695	T10V118H1S1L2	0.670
T5V118H1S2L2	0.456	T10V118H1S2L2	0.426
T5V118H5S1L2	0.370	T10V118H5S1L2	0.351
T5V118H5S2L2	0.669	T10V118H5S2L2	0.650
T5V236H1S1L2	0.650	T10V236H1S1L2	0.633
T5V236H1S2L2	0.719	T10V236H1S2L2	0.676
T5V236H5S1L2	0.650	T10V236H5S1L2	0.406
T5V236H5S2L2	0.721	T10V236H5S2L2	0.711

(Peralta et al., 2009) and secondly because the Tu parameter is an area averaged quantity treating all the jets as a single equivalent flow.

Fig. 8 shows that S, L and V affected the Tu profiles. Also, the effect of the refrigerant temperature on the profiles was negligible. In general, an increase in L produces higher values of Tu in the domain. This could be due to the existence of a larger volume of fluid with low velocity dissipating the jet energy to the surroundings. In the case of L = 6 cm (*i.e.* one sphere), the effect of the sphere on the fluid flow is similar to a case of a free jet (Deo et al., 2007; Ball et al., 2012). In this case, the presence of the sphere did not affect appreciably the Tu profiles. On the other hand, when L = 2 cm (*i.e.* 13 spheres), the Tu profiles show an initial increment until they reach the sphere array. This behavior produced higher values of Tu in the region between by the orifices and the spheres for the case of H = 5 cm. Consequently, the effect of S on Tu was observed when H = 5 cm.

Table 3 shows the $\langle Tu \rangle$ values calculated for all conditions. In general, the $\langle Tu \rangle$ values were affected in a similar manner by the geometric and operative variables as it was observed for Tu. The variables that most affected $\langle Tu \rangle$ were S, V and L (in that order of importance). Basically, an increase in S, V and L produced an increase in $\langle Tu \rangle$. As mentioned earlier, those increments allow the existence of larger zones with fluid recirculation. This behavior facilitates the dissipation of the jet energy into eddies producing an increase in the turbulence levels. Finally, the refrigerant temperature and the separation between the orifice plate and the spheres arrays shown a negligible effect on $\langle Tu \rangle$.

3.1.4. Pressure coefficient

The pressure coefficient (Cp) profiles as a function of the position on the sphere surface are shown in Fig. 9. In general, the profiles showed a maximum in the forward stagnation point of the spheres, followed by a minimum and/or second maximum in the zone of $30° < \varphi < 90°$ and an approximately constant value in the rear part of the spheres. Fig. 9 shows that the parameter that most influenced the Cp profiles was H followed by S. In the case of H = 1 cm (Fig. 9a and c), the first maximum was in the range of 0.6 (S = 2 cm) to 1 (S = 1 cm). This difference could be explained because when the jets are closer with each other (S = 1 cm), they tend to dissipate less energy with their surroundings because of the similarity of the velocities that produces a smaller deceleration of the fluid jet compared with the case of S = 2 cm. It can be observed that for S = 1 cm, the second maximum appeared in $\varphi \sim 50$–$60°$ due to the impingement of the jets adjacent to the jets that are collinearly placed with each sphere. In the case of S = 2 cm, the profiles were similar to the ones obtained by Peralta et al. (2010) for a system with a jet impinging collinearly a static sphere and by Lee et al. (1997) for an static hemisphere impinged by a single jet. This behavior could indicate that the spacing of S = 2 cm produces a similar effect of what a single jet produces in terms of pressure on the spheres. On the other hand, when H = 5 cm (Fig. 9b and d), the profiles were almost constant, showing that the energy of the jet was mainly dissipated to the surrounding fluid and the impingement is distributed more uniformly on the sphere surfaces. Again, higher values of Cp are found for S = 1 cm

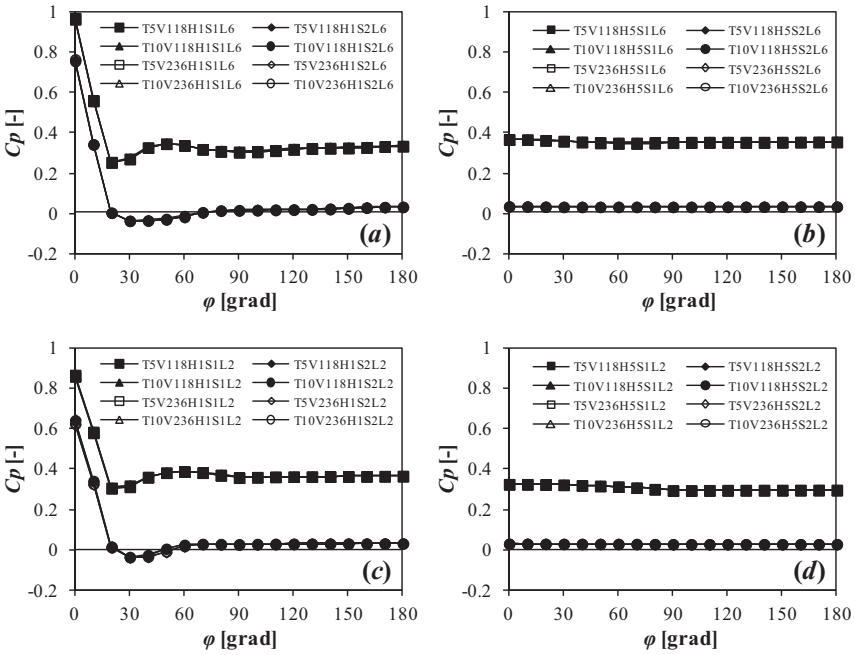

Fig. 9. Pressure coefficient profiles (*Cp*) as a function of the angular position on the sphere surface for the studied conditions. (a) $L = 6$ cm and $H = 1$ cm, (b) $L = 6$ cm and $H = 5$ cm, (c) $L = 2$ cm and $H = 1$ cm, and (d) $L = 2$ cm and $H = 5$ cm.

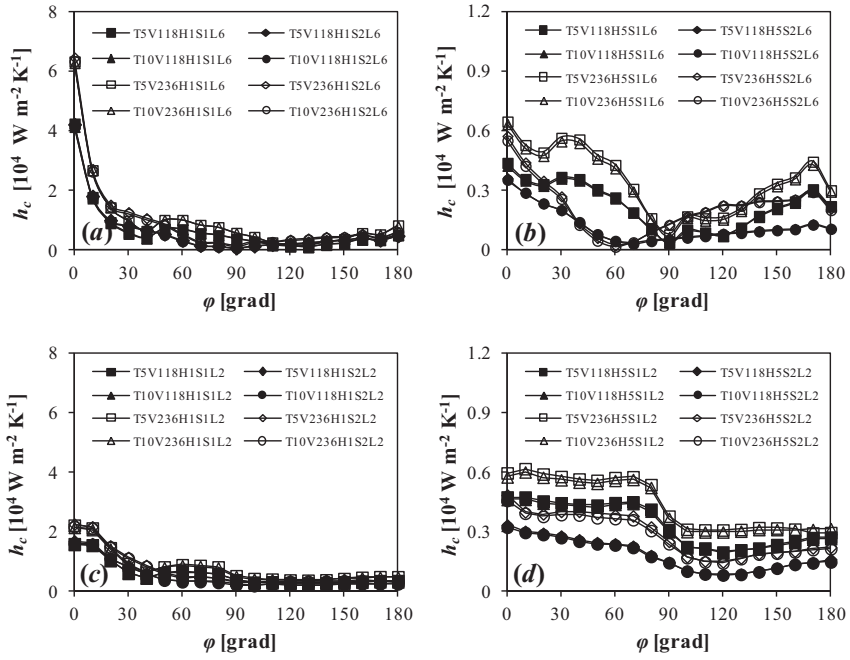

Fig. 10. Profiles of the local values of the surface heat transfer coefficient as a function of the angular position for the studied conditions evaluated at $t = 2$ s. (a) $L = 6$ cm and $H = 1$ cm, (b) $L = 6$ cm and $H = 5$ cm, (c) $L = 2$ cm and $H = 1$ cm, and (d) $L = 2$ cm and $H = 5$ cm.

compared with $S = 2$ cm. Finally, the refrigerant temperature, the average fluid velocity at the orifices and the separation between the spheres had a negligible effect on the *Cp* profiles.

3.1.5. Surface heat transfer coefficient

The profiles of the local surface heat transfer coefficient (h_c) as a function of the position on the sphere surface are showed in Fig. 10 for all conditions at a simulation time of 2 s. This time was selected due to the quasi-asymptotic nature of the h_c profiles exhibited after that time (profiles not showed). In general, the profiles of h_c presented a maximum in the forward stagnation point of the spheres, then a decrease until in some cases reach a minimum at $\varphi \approx 20$–$40°$, next a plateau or a second maximum at $\varphi \approx 40$–$70°$ followed by a decrease until reach another minimum in the equator zone ($70° < \varphi < 120°$). Finally, an increase of h_c is observed at the rear part of the sphere mainly due to the recirculation flow.

The parameter that most influenced the h_c profiles was *H*, followed by *L* and *S*. When $H = 1$ cm, the local values of h_c were higher than for $H = 5$ cm. In this case, a pronounced maximum is observed at the forward stagnation point due mainly to the small time that the jet has to dissipate its energy as turbulence (Fig. 8). A similar effect due to a second set of adjacent jets produces a much lower

Table 4
Values of h_c^* for the studied conditions.

Condition	h_c^* (W m^{-2} K^{-1})	Condition	h_c^* (W m^{-2} K^{-1})
T5V118H1S1L6	3632	T10V118H1S1L6	3561
T5V118H1S2L6	3004	T10V118H1S2L6	2942
T5V118H5S1L6	1674	T10V118H5S1L6	1637
T5V118H5S2L6	1042	T10V118H5S2L6	1036
T5V236H1S1L6	5217	T10V236H1S1L6	5050
T5V236H1S2L6	4340	T10V236H1S2L6	4224
T5V236H5S1L6	2591	T10V236H5S1L6	3073
T5V236H5S2L6	1283	T10V236H5S2L6	1272
T5V118H1S1L2	4468[a]	T10V118H1S1L2	4087[a]
T5V118H1S2L2	3267[a]	T10V118H1S2L2	3163[a]
T5V118H5S1L2	3152[a]	T10V118H5S1L2	3099[a]
T5V118H5S2L2	1570[a]	T10V118H5S2L2	1562[a]
T5V236H1S1L2	6093[a]	T10V236H1S1L2	5916[a]
T5V236H1S2L2	4789[a]	T10V236H1S2L2	4655[a]
T5V236H5S1L2	4160[a]	T10V236H5S1L2	4072[a]
T5V236H5S2L2	2338[a]	T10V236H5S2L2	2279[a]

[a] Value averaged considering the 13 spheres.

second maximum observed at $\varphi \approx 40$–$70°$. In the case of $H = 5$ cm, both maximum values present a similar height due mainly to the energy dissipated to generates turbulence that produce jets with higher diameters near the sphere arrays (Figs. 6 and 7). The presence of the second maximum at $H = 5$ cm depends on the values of S and L. When $S = 2$ cm, the second maximum is lost. This could be explained due to the spheres are affected mainly by the jets that are located directly below. Furthermore, when $L = 2$ cm, a plateau is formed due to the smooth change between the first and second maxima. In this case, the probability of impingement at the front part of the spheres by the flow jet is increased due to the higher number of spheres distributed in the domain. In all cases, the relative increment of the local values after the minimum depends on H, L and S. Also, the profiles of h_c are more uniform (*i.e.* similar profiles at front and rear). The slope of h_c after the minimum is increased for low values of S and high values of L. Again, this is because the amount of the jet energy that reaches the rear part of the spheres.

In all cases, the average fluid velocity at the orifices produced scaled h_c profiles (higher velocities produced higher local values). The refrigerant temperature had no appreciable effect on the profiles. Similar results were observed previously by Peralta et al. (2010) in a similar HF system composed by a single sphere impinged by a single jet.

Table 4 shows the values of h_c^* calculated from the spheres central temperature. In general, the geometric and operative variables affected similarly the values of h_c^* and h_c. The variables that mainly affected h_c^* were H, S, V and L (in this order of importance). An increase in V and a decrease in H, S and L, produce an increase in h_c^*. This behavior was partially observed by Robinson and Schnitzler (2007) for a jet impinging system. The effect of T on h_c^* was negligible. It should be recalled that the values of h_c^*, being an averaged quantity in space and time (Peralta et al., 2010), are representative values of the heat transfer that take place in every studied condition and are easier to compare against experimental data.

3.1.6. Nusselt correlation

Eq. (7) shows the obtained correlation along with its range of validity. The coefficient $a_{3,j}$ was taken as 0.4 based on Peralta et al. (2009) and Tie et al. (2011). This value is similar to the one found when it was included in the fitting procedure ($a_{3,j} \cong 0.41$). The comparison between the simulated $Nu_j/Pr^{0.4}$ values and the ones calculated using Eqs. (7) and (8) are shown in Fig. 11. The mean percentage error of fitting was lower than 15% in both cases and was considered as good.

$$Nu_{ave} = 2.024 Re^{0.508} Pr^{0.4} (H/d)^{-0.372} (S/d)^{-0.456} (L/d)^{-0.194} \quad (7)$$

$$Nu_{stg} = 1.372 Re^{0.551} Pr^{0.4} (H/d)^{-1.421} (S/d)^{-0.033} (L/d)^{0.884} \quad (8)$$

where $40 < Nu_{ave} < 230$, $120 < Nu_{stg} < 2420$, $6000 < Re < 15000$, $23 < Pr < 29$, $3.3 < H/d < 16.6$, $3.3 < S/d < 6.6$, $6.6 < L/d < 20$.

The coefficients $a_{2,ave}$ and $a_{2,stg}$, related to Re, resulted ~0.5. This could imply that the flow around the spheres was laminar (Elison and Webb, 1994; Webb and Ma, 1995; Zhou and Ma, 2006). The coefficients $a_{4,j}$ (related to H/d) and $a_{5,j}$ (related to S/d) presented negative values. This negative nature was found in literature for the case of $a_{4,j}$ in systems with impinging single and multiple jets on flat surfaces and cylinder arrays and $H/d > 5$ (Chang et al., 1995; Webb and Ma, 1995; Anwarullah et al., 2011), and for impinging array of jets on flat surfaces in the case of $a_{5,j}$ (Huber and Viskanta, 1994). It is noteworthy to mention that the coefficients $a_{2,ave}$, $a_{4,ave}$ and $a_{5,ave}$ of Eq. (7) for Nu_{ave} are similar to those found by Robinson and Schnitzler (2007) for a submerged and confined jet array impinging on to a flat surface. Also, $a_{1,stg}$ and $a_{2,stg}$ are similar to those found by Lee et al. (1997) for Nu_{stg} for jet impingement on a hemispherical surface.

3.2. Heat and mass transfer in the food domain

3.2.1. Average NaCl concentration profiles

The mass transfer in the food domain was studied using average NaCl concentration (C_{NaCl}) profiles (Peralta et al., 2012). In all cases (Fig. 12a), the temperature of the refrigerant was the variable that most affected the C_{NaCl} profiles. The rest of the variables (average velocity of the refrigerant fluid, distance between the center of the orifices and the distance between the orifices and sphere stagnation points), had a negligible effect on the profiles. This behavior could be explained because both, the diffusion coefficient and the freezing process are mainly affected by temperature. In general, an increase in temperature produces an increase in the diffusion coefficient of NaCl in water. Also, an increased T causes a smaller

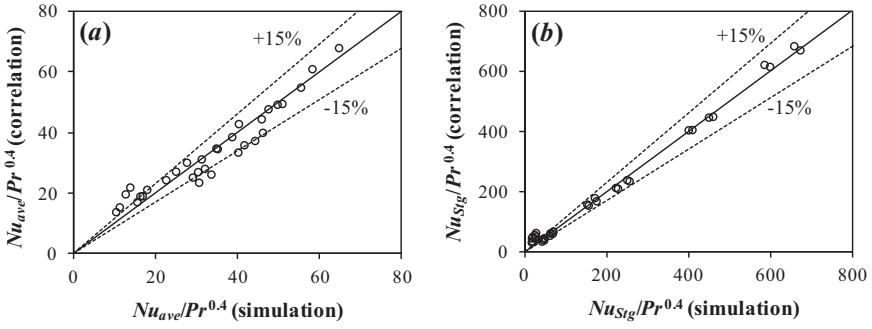

Fig. 11. Comparison of simulated and predicted Nusselt values. (a) $Nu_{ave}/Pr^{0.4}$ values (Eq. (7)) and (b) $Nu_{stg}/Pr^{0.4}$ values (Eq. (8)). Dashed lines correspond to a mean percentage average error of ±15%.

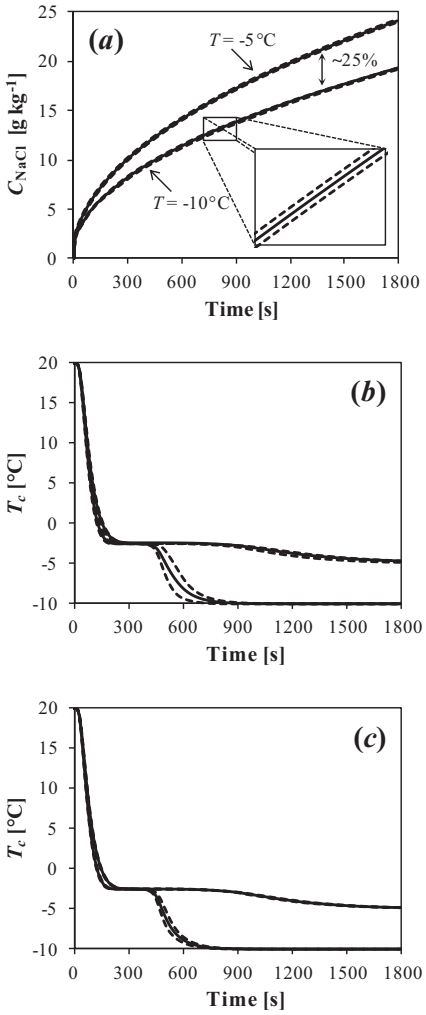

Fig. 12. (a) Average NaCl concentration profiles as a function of time for the studied conditions and profiles of the average temperature of the geometric center of the spheres (solid line) as a function of time for the studied conditions. (b) $L = 6$ cm and (c) $L = 2$ cm. The dashed lines correspond to the standard deviation observed for each condition.

difference between T and the initial freezing point of the food product. This small difference causes the freezing velocity to decrease and the exposure times of the unfrozen parts of the food to a certain temperature to increase leading to an increase in the diffusion of the solutes towards the center. It is important to mention that a 25% increment in the solute gain was observed for the spheres at $T = -5$ °C relative to $T = -10$ °C.

3.2.2. Central temperature profiles and freezing times

The profiles of the temperature at the geometric center of the spheres (T_c) (Fig. 12b and c) were used as one of the representative parameters used to study the heat transfer in the food domain (Peralta et al., 2012). Based on T_c, a characteristic freezing time was defined necessary for the center to reach −4 °C. To compare the freezing times, a relative freezing time parameter (t_R) was defined as the ratio of the freezing time at a certain condition to the smaller freezing time obtained (*i.e.* t_R evaluated at T10V236H1S1L6).

Fig. 13 shows the average T_c profiles as a function of time for the two refrigerant temperatures studied. The dashed lines represent the range of temperature profiles obtained varying the rest of the operative variables. Based on this information, the T_c profiles were mainly affected by T, whereas the rest of the variables had a negligible impact. A similar behavior was observed for t_R. Averaging, an increment of 5 °C produced an increase of approximately 1.7 times the values of t_R. Furthermore, an increase of 1 cm in S and 4 cm in H, and a decrease of 1.18 m s^{-1} in V and 4 cm in L, produced an increment of approximately 10% in t_R. The combined effect of the operative variables, comparing t_R at T10V236H1S1L6 (most favorable condition for heat transfer) to t_R at T5V11H5S2L6 (least favorable condition for heat transfer), produced an increment of 3.16 times the values of t_R.

4. Conclusions

A study of the effect of the number of orifices in a square array and operative conditions such as the refrigerant temperature, the distance between the plate with the orifices and the plane of the stagnation point of the spheres, the average velocity of the fluid at the orifices, and the distance between the geometric center of the spheres, on the transport phenomena in a freezing process of

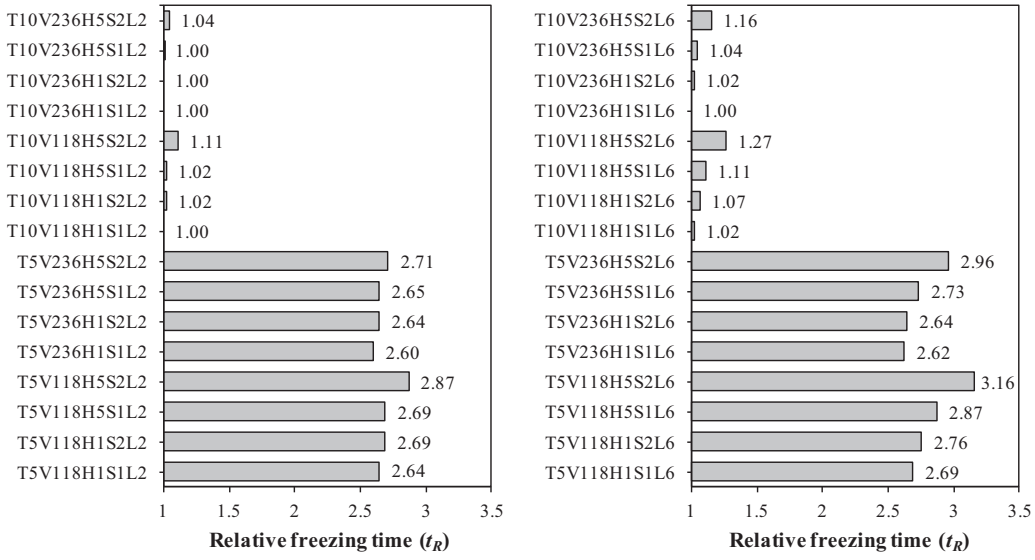

Fig. 13. Relative freezing times for the studied conditions. The condition adopted as reference was T10V236H1S1L6.

static potato spheres in a hydrofluidization system was carried out. The work consisted in the estimation of the transport phenomena through a mathematical modeling by separating the study of the transfer within the refrigerant domain and the food domain. This was possible due to the difference in orders of magnitude between momentum transfer in the refrigerant (medium with high fluid velocities and high turbulence levels) and the heat and mass transfer.

On the one hand, momentum, energy and mass (continuity) balances were solved in the refrigerant fluid domain using computational fluid dynamics. Representative variables of the studied transfers such as local and averaged values of the surface heat transfer coefficient, pressure coefficient, local and averaged turbulence levels, velocity contours and streamlines. On the other hand, a mathematical model developed in previous hydrofluidization works was used to study the freezing process. The representative parameters studied were the temperature at the geometric center of the spheres, the freezing time and the averaged NaCl concentration profiles. It should be pointed out that both modeling approaches (in the refrigerant and food domains) were developed and validated in previous works.

The variable that most affected the profiles of h_c, h_c^*, Cp, Tu and $\langle Tu \rangle$ was the distance between the plate with orifices and the plane of the stagnation points of the spheres (H). The second operative variable, in order of importance, was the distance between the geometric center of the orifices (S) followed by the average fluid velocity at the orifices (V) and the distance between the geometric center of the spheres (L). The refrigerant temperature had a negligible effect on the mentioned profiles. In general, a decrease in H, S and L, and an increase in V, produced and increment in the values of h_c, h_c^*, Cp, Tu and $\langle Tu \rangle$. These results showed that the transport phenomena in the refrigerant domain may be greatly influenced by the geometric variables of the system. Regarding the transfer within the food, the most influencing variables on the temperature profiles, freezing times and average NaCl concentration were the refrigerant temperature, while S, V, H and L had a secondary and similar effect on the mentioned profiles. In general, an increase in temperature caused an increase in the solute gain and the freezing times. The variables S, V, H and L had no noticeable influence on the average NaCl concentration profiles. Nevertheless, an appreciable effect on the freezing times was observed (t_R increased as S and H increased and V and L decreased).

This study shows the relative importance of the geometric operative variables on the transport phenomena that take place in a hydrofluidization system during a freezing process. These results will allow proposing new operative conditions to be studied, such as different arrays of spheres and orifices, and mobile foods.

Acknowledgments

This research was supported partially by Universidad Nacional del Litoral (Santa Fe, Argentina), Consejo Nacional de Investigaciones Científicas y Técnicas (CONICET, Argentina), and Agencia Nacional de Promoción Científica y Tecnológica (ANPCyT, Argentina).

References

Anwarullah, M., Rao, V.V., Sharma, K.V., 2011. Effect of nozzle spacing on heat transfer and fluid flow characteristics of an impinging circular jet in cooling of electronic components. Int. J. Therm. Environ. Eng. 4, 7–12. http://dx.doi.org/10.5383/ijtee.04.01.002.

Ball, C.G., Fellouah, H., Pollard, A., 2012. The flow field in turbulent round free jets. Prog. Aerosp. Sci. 50, 1–26. http://dx.doi.org/10.1016/j.paerosci.2011.10.002.

CFX, 2006. ANSYS CFX-solver theory guide. In: ANSYS CFX Help. ANSYS Inc., Canonsburg.

Chang, C.T., Kojasoy, G., Landis, F., Downing, S., 1995. Confined single- and multiple-jet impingement heat transfer—I. Turbulent submerged liquid jets. Int. J. Heat Mass Transfer 38, 833–842. http://dx.doi.org/10.1016/0017-9310(94)00202-7.

Deo, R.C., Mi, J., Nathan, G.J., 2007. The influence of nozzle-exit geometric profile on statistical properties of a turbulent plane jet. Exp. Therm. Fluid Sci. 32, 545–559. http://dx.doi.org/10.1016/j.expthermflusci.2007.06.004.

Draksler, M., Ničeno, B., Končar, B., Cizelj, L., 2014. Large eddy simulation of multiple impinging jets in hexagonal configuration – mean flow characteristics. Int. J. Heat Fluid Flow 46, 147–157. http://dx.doi.org/10.1016/j.ijheatfluidflow.2014.01.005.

Elison, B., Webb, B.W., 1994. Local heat transfer to impinging liquid jets in the initially laminar, transitional, and turbulent regimes. Int. J. Heat Mass Transfer 37, 1207–1216. http://dx.doi.org/10.1016/0017-9310(94)90206-2.

Fikiin, A.G., 1992. New method and fluidized water system for intensive chilling and freezing of fish. Food Control 3, 153–160. http://dx.doi.org/10.1016/0956-7135(92)90100-O.

Fikiin, K., 2008. Frozen Food Science and Technology. Blackwell Pub, Oxford, Ames, Iowa.

Geers, L.F.G., Tummers, M.J., Hanjalic, K., 2004. Experimental investigation of impinging jet arrays. Exp. Fluids 36, 946–958. http://dx.doi.org/10.1007/s00348-004-0778-2.

Geers, L.F.G., Tummers, M.J., Hanjalić, K., 2005. Particle imaging velocimetry-based identification of coherent structures in normally impinging multiple jets. Phys. Fluids 17, 055105. http://dx.doi.org/10.1063/1.1900804.

Huber, A.M., Viskanta, R., 1994. Effect of jet–jet spacing on convective heat transfer to confined, impinging arrays of axisymmetric air jets. Int. J. Heat Mass Transfer 37, 2859–2869. http://dx.doi.org/10.1016/0017-9310(94)90340-9.

Kuroki, M., Ookawara, S., Ogawa, K., 2009. A high-fidelity CFD model of methane steam reforming in a packed bed reactor. J. Chem. Eng. Jpn. 42, s73–s78. http://dx.doi.org/10.1252/jcej.08we256.

Lee, D.H., Chung, Y.S., Kim, D.S., 1997. Turbulent flow and heat transfer measurements on a curved surface with a fully developed round impinging jet. Int. J. Heat Fluid Flow 18, 160–169. http://dx.doi.org/10.1016/S0142-727X(96)00136-1.

Olsson, E.E.M., Ahrné, L.M., Trägårdh, A.C., 2004. Heat transfer from a slot air jet impinging on a circular cylinder. J. Food Eng. 63, 393–401. http://dx.doi.org/10.1016/j.jfoodeng.2003.08.009.

Peralta, J.M., Rubiolo, A.C., Zorrilla, S.E., 2007. Prediction of heat capacity, density and freezing point of liquid refrigerant solutions using an excess Gibbs energy model. J. Food Eng. 82, 548–558. http://dx.doi.org/10.1016/j.jfoodeng.2007.03.010.

Peralta, J.M., Rubiolo, A.C., Zorrilla, S.E., 2009. Design and construction of a hydrofluidization system. Study of the heat transfer on a stationary sphere. J. Food Eng. 90, 358–364. http://dx.doi.org/10.1016/j.jfoodeng.2008.07.004.

Peralta, J.M., Rubiolo, A.C., Zorrilla, S.E., 2010. Mathematical modeling of the heat transfer and flow field of liquid refrigerants in a hydrofluidization system with a stationary sphere. J. Food Eng. 99, 303–313. http://dx.doi.org/10.1016/j.jfoodeng.2010.03.003.

Peralta, J.M., Rubiolo, A.C., Zorrilla, S.E., 2012. Mathematical modeling of the heat and mass transfer in a stationary potato sphere impinged by a single round liquid jet in a hydrofluidization system. J. Food Eng. 109, 501–512. http://dx.doi.org/10.1016/j.jfoodeng.2011.10.032.

Robinson, A.J., Schnitzler, E., 2007. An experimental investigation of free and submerged miniature liquid jet array impingement heat transfer. Exp. Therm. Fluid Sci. 32, 1–13. http://dx.doi.org/10.1016/j.expthermflusci.2006.12.006.

Tie, P., Li, Q., Xuan, Y., 2011. Investigation on the submerged liquid jet arrays impingement cooling. Appl. Therm. Eng. 31, 2757–2763. http://dx.doi.org/10.1016/j.applthermaleng.2011.04.048.

Verboven, P., Scheerlinck, N., Nicolaï, B.M., 2003. Surface heat transfer coefficients to stationary spherical particles in an experimental unit for hydrofluidisation freezing of individual foods. Int. J. Refrig. 26, 328–336. http://dx.doi.org/10.1016/S0140-7007(02)00110-X.

Webb, B.W., Ma, C.-F., 1995. Single-phase liquid jet impingement heat transfer. In: Advances in Heat Transfer. Elsevier, pp. 105–217.

Wilcox, D.C., 2006. Turbulence Modeling for CFD, third ed. DCW Industries, La Cãnada.

Zhou, D.W., Ma, C.F., 2006. Radial heat transfer behavior of impinging submerged circular jets. Int. J. Heat Mass Transfer 49, 1719–1722. http://dx.doi.org/10.1016/j.ijheatmasstransfer.2005.10.021.

Zorrilla, S.E., Rubiolo, A.C., 2005a. Mathematical modeling for immersion chilling and freezing of foods. J. Food Eng. 66, 329–338. http://dx.doi.org/10.1016/j.jfoodeng.2004.03.026.

Zorrilla, S.E., Rubiolo, A.C., 2005b. Mathematical modeling for immersion chilling and freezing of foods. J. Food Eng. 66, 339–351. http://dx.doi.org/10.1016/j.jfoodeng.2004.03.027.